Virtual Optical Modes for Quantum Illumination

Marco Lanzagorta
US Naval Research Laboratory
Washington, DC 20375
marco.lanzagorta@nrl.navy.mil

Jeffrey Uhlmann
University of Missouri - Columbia
Columbia, MO 65211
uhlmannj@missouri.edu

***Abstract*—Quantum-based sensing offers theoretical advantages over traditional classical alternatives. In the case of active radio-frequency quantum sensors, however, there exist several practical challenges, the most significant of which is the fast and efficient generation of entangled microwave photons. In a previous paper we proposed a method, called virtual modes, for mitigating this limitation by using a distributed architecture of quantum sensor units to synthetically increase the effective number of distinguishable modes available for target detection. Although this architecture was shown to incur an increase in noise cross-contamination, we showed that judicious sensor configurations can mitigate this effect. In this paper we examine more sophisticated cross-noise statistical models that permit the number and spatial distribution of sensors to be optimized to further reduce the net detection error probability of the proposed approach.**

I. Introduction

In theory, quantum information and quantum sensing offer potential advantages over classical alternatives. In this paper our interest is in quantum object-detection sensors/systems that determine attributes of observed objects by illuminating them with microwave photons [1]. As discussed in [2], the practical applications of such radio-frequency active sensors are limited by the rate at which a microwave illumination device can generate M independent mode pairs, where M is the product of the time length of the signal pulse and the bandwidth. In the case of an X-band quantum sensor (approximately 4 GHz with 1 ms-length pulses) the value of M is several orders of magnitude too small for most practical applications, so a method for creating additional *virtual modes* [2] was developed. In this paper we extend and analyze the method of virtual modes.

II. Quantum Illumination

Assuming Gaussian quantum illumination, the detection error probability (DEP) can be characterized using standard techniques from quantum optics [3], [4]. In the low-brightness, high-noise, low-reflectivity regime it can be established that $N_s \ll 1$, $N_b \gg 1$, and $\kappa \ll 1$, where N_s is the average number of photons per mode, κ is the reflectivity, and N_b is the average background number of photons. Under these conditions, and assuming no ability to exploit knowledge of the likelihood that a target is present or not, the detection error probability, DEP=ϵ_q, for an entangled-photon detector can be expressed as:

$$\epsilon_q \leq P_q \equiv \frac{e^{-M\kappa N_s/N_b}}{2} = \frac{e^{-SNR}}{2} \tag{1}$$

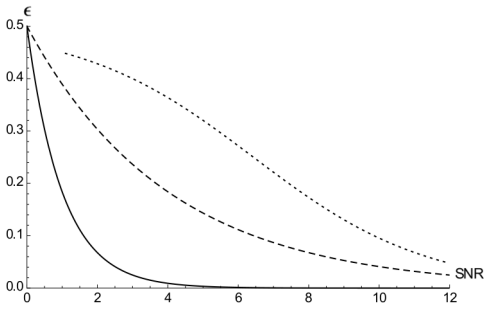

Fig. 1. Detection error probability upper bound ϵ for $M = 10^9$ entangled photon states (P_q - solid line), coherent unentangled photon states (P_l - dashed line), and a coherent integration of classical radar pulses (P_c - dotted line), with respect to the signal-to-noise ratio (SNR).

where M is the number of signal pulses emitted to illuminate the target [3]. In this paper we will approximate $SNR \approx \kappa N_s/N_b$.

This formulation of detection error combines both false-positive and false-negative cases into a single quantity. For example, in the ideal case of high signal (i.e., the number $M\kappa N_s$ of reflected photon detections is large) and minimal background noise (i.e., $N_b \approx 0$), the detection error probability approaches 0. However, as $M\kappa N_s$ becomes very small, or as the average number of background photons N_b (i.e., noise) becomes very large, the detection error probability approaches the zero-information limit of $\frac{1}{2}$, i.e., the detection is equally likely to be real or spurious.

The detection error probability ϵ_l for a coherent light sensor is bounded by:

$$\epsilon_l \leq P_l \equiv \frac{e^{-M\kappa N_s/(4N_b)}}{2} = \frac{e^{-SNR/4}}{2} \tag{2}$$

Figure 1 shows the comparative performance of the three types of sensor based on the detection error probability upper bound. For concreteness of discussion, the key variables are taken to have the values $N_s = 10^{-4}$, $N_b = 10^4$, and $\kappa = 0.1$, which are broadly within the range of typical [5]. It can be observed that in the low signal-to-noise ratio and low-brightness regime the quantum sensor performs significantly better than the coherent and classical sensors, which is consistent with previously-reported results [3], [5]. However, if the SNR is too small, then all sensors have a detection error probability of nearly 1/2, which is equivalent to zero discrimination capability. Similarly, if the SNR is sufficiently large then then

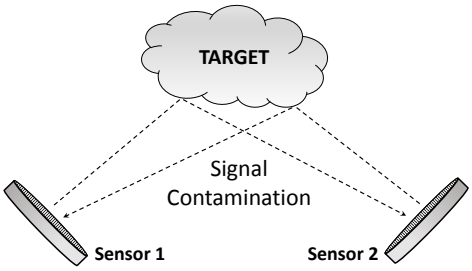

Fig. 2. A system composed of two sensors will increase the number of distinguishable modes. However, each sensor will generate photons that may be received as noise by the other. The result of this cross-contamination is an effective increase in the background noise experienced by each sensor and, consequently, the net background noise of the joint system.

the detection error probability approaches zero for all sensors and again there is no ability for a quantum sensor to perform better than the coherent or the classical system. It can be shown that, for the case under consideration, the optimal number of signal pulses M is about $M \approx 10^9$.

III. Virtual Modes via Distributed Detection and Fusion

The number of distinguishable modes (M) available for a single illuminator-detector is $M = W \times T$, where W is the bandwidth and T the period of the signal. Assuming that a quantum sensor operates in the X-band at 10 GHz, and works with a 40% fractional bandwidth, then the bandwidth is approximately 4 GHz. If the signal pulses are emitted with a period of 1 ms then $M \approx 4 \times 10^3$, i.e., much less than the $M \approx 10^9$ required in the previous example (Fig. 1). In general, the number of distinguishable modes available in the primary radio-spectrum bands is impractically small [2].

To overcome the constraints imposed by small M, we propose a distributed architecture of quantum sensors for which the effective size of M can be increased [2]. A different approach to this problem is the use of multiple-input multiple-output channels using beam-splitters [6].

To illustrate the virtual modes concept, consider the case in which N quantum sensors are spatially distributed. In other words, the system of N sensors operates with efficiency equivalent to having MN distinguishable modes, i.e., it exploits an additional $(N-1)M$ virtual modes.

As N is increased, however, the effective size of the background noise parameter N_b for each sensor will increase due to the additional photons errantly received from the other $N-1$ sensors (Fig. 2). Letting α denote this *cross-contamination fraction*, the background noise is increased to $N_b + \alpha(N-1)M\kappa N_s$, which in the large N limit leads to a total detection error probability:

$$\pi \approx \frac{1}{2} e^{-\frac{MN\kappa N_s}{N_b + \alpha(N-1)M\kappa N_s}} \approx \frac{1}{2} e^{-\frac{SNR}{1+\alpha SNR}} \qquad (3)$$

where $0 \leq \alpha \leq 1$. A key fact is that the numerator of the exponent is multiplicatively increased by the number of sensors N whereas the cross-noise enters additively in the denominator. The relative effects of N and α on the detection error probability of the system are depicted in Fig. 3.

It should be noted that Eqn. (3) does not represent an effective detection probability bound for the system as a whole and thus do not make any assumptions about how the signals or decisions from the multiple sensors are combined/fused, i.e., the system as a whole is treated simply as a single virtual sensor. However, it has been shown in the traditional radar setting that the fusion process can sometimes exploit additional information, e.g., topological constraints, to obtain further improvements in detection performance [7].

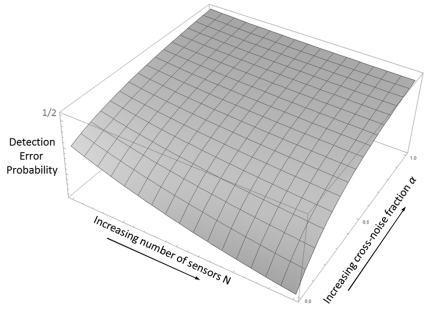

Fig. 3. The detection error probability of the system is reduced with increasing N and $\alpha \ll 1$. Conversely, as α increases relative to N the detection error probability approaches the zero-information limit of 1/2.

Figure 4 shows the performance of a classical sensor (solid line) and a quantum sensor system with zero ($\alpha = 0.5$, dashed line), medium ($\alpha = 0.5$, dotted line), and maximal ($\alpha = 1$, dash-dotted line) cross contamination. Clearly, as the cross-contamination increases, so does the detection error probability.

However, a quantum advantage occurs as long as the quantum error detection probability is smaller than the classical detection error probability: $\pi_q < \pi_c$, which means that $\alpha < 3/SNR$. For the case of maximal contamination, breakeven happens at $SNR = 3$, and for $\alpha = 0.5$ the breakeven is at $SNR = 6$. This behavior is shown in Figure 4. Notice that, if $\alpha = 1$ and $SNR > 3$, then the classical sensor system performs better than the quantum sensor. Classical outperformance of the quantum sensor is also observed when $\alpha = 0.5$ and $SNR > 6$.

Therefore, this analysis makes clear that there is a region in the low signal-to-noise ratio limit where quantum sensing augmented with virtual modes will always outperform classical and coherent sensing, even in the presence of maximal cross contamination.

IV. Distributed Sensing Nodes

The simple two-sensor example of Figure 2 suggests that the level of cross noise contamination can be affected by the configuration of sensors. For example, if two sensors are oriented in co-specular directions with respect to an illuminated object then photons from each will contaminate the other to a greater extent, while the signal photons received by

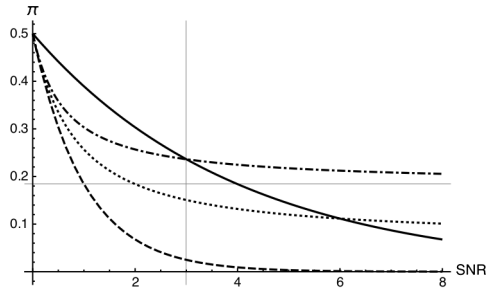

Fig. 4. Classical (solid line) and quantum detection error probability π as a function of the signal-to-noise ratio for $\alpha = 0$ (dashed line), $\alpha = 0.5$ (dotted line), $\alpha = 1$ (dot-dashed line). Also shown is the asymptotic limit for the detection error probability with the maximal cross contamination $\alpha = 1$ for arbitrarily large SNR (horizontal grid-line).

each sensor will be relatively small. In this and the following section we partially address these issues through examination of simple first-order (pairwise and symmetric-with-respect-to-target) sensor configuration dependencies.

The bistatic quantum cross section of a rectangular target of size a is given by:

$$\sigma(\theta_i, \theta_s) = \frac{4a^2}{\pi} |\cos\theta_i| \frac{\sin^2\left(ka\left(\sin\theta_s - \sin\theta_i\right)\right)}{\left(\sin\theta_s - \sin\theta_i\right)^2} \quad (4)$$

where $k = 2\pi/\lambda$ is the wave number, and θ_i and θ_s are the angles with respect to the emitter and the receiver, respectively [8]. By setting $\theta \equiv \theta_i = \theta_s$, we obtain the cross section for a monostatic sensor:

$$\sigma(\theta) = \frac{4\pi a^4}{\lambda^2} |\cos\theta_i| \left(\frac{\sin\left(ka\sin\theta\right)}{ka\sin\theta}\right)^2 \quad (5)$$

Let us recall that the detection error probability for a single quantum sensor with $SNR = s$ is given by $\pi_q = e^{-s}/2$. Then, for N sensors with the exact same SNR we have:

$$\pi_q^{(N)} = \prod_{i=1}^{N} \pi_q = \frac{1}{2} e^{-s \cdot N}. \quad (6)$$

However, assuming the same SNR for all is clearly unrealistic. For example, in the case of two sensor located at angles θ_1 and θ_2 with respect to the normal of the target, we can write:

$$\begin{aligned} s_1 &= \frac{M\kappa N_s\ \sigma(\theta_1)}{N_b + M\kappa N_s\ \sigma(\theta_1, \theta_2)} \\ s_2 &= \frac{M\kappa N_s\ \sigma(\theta_2)}{N_b + M\kappa N_s\ \sigma(\theta_2, \theta_1)} \end{aligned} \quad (7)$$

This expressions conveys the idea that sensor 1 receives a fraction$\sigma(\theta_1)$ of its own signal photons and a fraction $\sigma(\theta_1, \theta_2)$ of the signal photons from sensor 2 which contribute to the noise count. And similarly for sensor 2. Therefore, the total detection error probability is given by:

$$\pi_q^{(2)} = \frac{1}{2} e^{s_1 + s_2}. \quad (8)$$

Similarly, for N sensors we have:

$$s_i = \frac{M\kappa N_s\ \sigma(\theta_i)}{N_b + M\kappa N_s\ \sum_{j \neq i} \sigma(\theta_i, \theta_j)} \quad (9)$$

which results in the total detection error probability:

$$\pi_q^{(N)} = \prod_{i=1}^{N} \pi_q^{(i)} = \frac{1}{2} e^{-\sum s_i} \quad (10)$$

Notice that, in the specific case when the sensors are closely clustered together with respect to the angle, $\theta_i \approx \theta_j\ \forall j$ and we get:

$$s_i \approx \frac{M\kappa N_s\ \sigma}{N_b + M\kappa N_s (N-1)\sigma} \quad (11)$$

which leads to a detection error probability given by Equation (3) for the case of maximal cross node contamination $\alpha = 1$.

V. Some Computational Results

Figure 5 shows the cross section of a rectangular target observed close to the specular direction, i.e., it is essentially a plate from the perspective of the sensor. Thus, we can expect a return signal even if the sensors are off the specular direction. We have assumed $a = 0.2m$ and $\lambda = 0.03m$.

Figure 6 shows the respective detection error probabilities for observations made by a system of two classical sensors and a system of two quantum sensors in the case of a maximally reflective plate ($\kappa = 1$). We have also used $M = 10^8$ and the typical values $N_s = 10^{-4}$ and $N_b = 10^4$. We have also assumed that the two sensors are at angles θ and $-\theta$ with respect to the normal to the target. We notice that, near the specular direction ($\theta \approx 0$), the performance of the quantum system is inferior due to cross noise contamination. However, the quantum system is superior when the location of the sensors is moved so that the angle of observation with respect to specular is increased. This crossover in performance occurs when degradation due to cross noise diminishes so that the intrinsically superior sensitivity of the quantum system yields a net advantage over the classical system.

Figure 7 shows results for the same scenario as Figure 6 except that the assumed reflectivity of the target has been dramatically reduced to $\kappa = 0.025$. This leads to reduced cross noise for the quantum system and allows it to outperform classical even when its sensors are configured near the specular direction. This suggests that the classical advantage shown in Figure 6 is largely due to the assumption of perfect target reflectivity (large SNR limit). More specifically, perfect reflectivity maximizes the average information received per photon transmitted by the classical system and at the same time maximizes cross noise contamination of the quantum system. Figure 7 by contrast shows that diminished target reflectivity reduces both the advantage of the classical system and the disadvantage of the quantum system. This results indicates that multi-static quantum sensing could detect targets off the specular direction much better than with classical sensors.

Figure 8 plots the difference of the classical and quantum detection error probabilities ($\pi_c - \pi_q$) from Figures 6 and 7 to characterize the relatively narrow regime in which classical outperforms quantum. This is done for the case of maximal (red) and small (blue) reflectivity. Thus, a positive value indicates that the quantum system is better. As explained

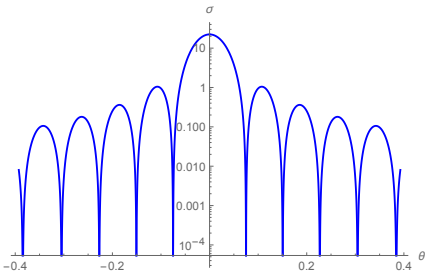

Fig. 5. Cross section of rectangular target near the specular direction.

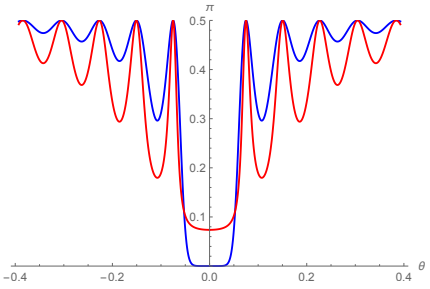

Fig. 6. Detection error probability for classical (blue) and quantum (red) sensing for a maximal reflectivity target.

before, the classical sensor is better only in the case of maximal reflectivity and near the specular direction. In all the other cases, the quantum system performs better than the classical.

Finally, in Figure 9 we show the case of the first quantum sensor observing the target at the specular direction ($\theta_1 = 0$), while the second is at angle θ with respect to the normal to the target. On the other hand, the classical sensor in the specular direction. In this case the quantum system always performs better than the classical sensor. And furthermore, the optimal position of the second quantum sensor is at the specular direction, even though in this position the cross contamination is maximal.

VI. Conclusions

In this paper we have discussed the method of virtual modes to mitigate the limitations imposed by practical sources of

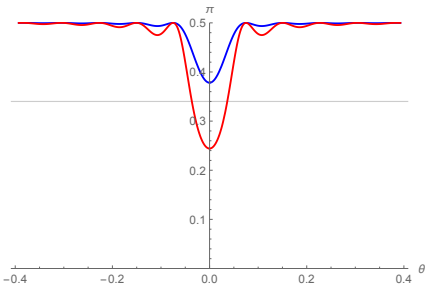

Fig. 7. Detection error probability for classical (blue) and quantum (red) sensing for a target with small reflectivity.

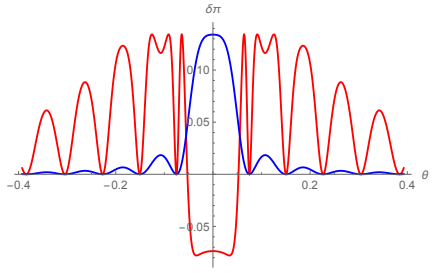

Fig. 8. Difference between classical and quantum detection error probabilities for a target with maximal (red) and small (blue) reflectivity.

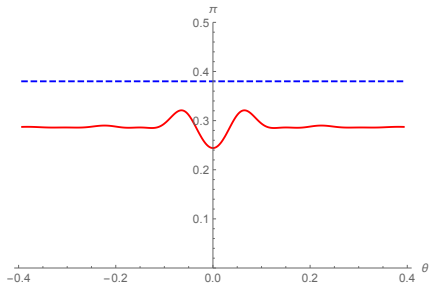

Fig. 9. Detection error probability for one quantum sensor fixed in the specular direction (blue) compared to the classical DEP (red) and the optimal quantum DEP (green).

entangled photons for distributed quantum sensing systems. We have argued that more sophisticated analysis is required to model the effects of sensor configuration on critical performance variables such as cross noise contamination. In fact, we presented results showing that there are scenarios in which a classical sensing system can outperform the proposed quantum-based system. However, further analysis suggests that the regime of classical superiority is relatively narrow and that a quantum-based system can offer significantly better performance in most scenarios outside that regime.

References

[1] M. Lanzagorta, *Quantum Radar*, Morgan & Claypool, 2011.

[2] M. Lanzagorta, J. Uhlmann, and Truc Le, "Improving Quantum Sensing with Virtual Modes," *Proc. Proc. SPIE Radar Sensor Technology XX*, Vol. 9829, May 2016.

[3] S. Hui-Tan, B.I. Erkmen, V. Giovannetti, S. Guha, S. Lloyd, L. Maccone, S. Pirandola, and J.H. Shapiro, "Quantum Illumination with Gaussian States", *Phys. Rev. Lett.* 101, 253601, 2008.

[4] S. Barzanjeh,S. Guha, C. Weedbrook, D. Vitali,J.H. Shapiro, and S. Pirandola, "Microwave Quantum Illumination," arXiv:1503.00189v1 [quant-ph], 28 Feb 2015.

[5] M. Lanzagorta, "Low-Brightness Quantum Radar", *Proceedings of the SPIE Defense, Security and Sensing: Radar Sensor Technology*, 2015.

[6] R. Janti, et.al., "Multiantenna Quantum Backscatter Communications", arXiv:1707.02560 [cs.IT], 2017.

[7] C. Rago, P. Willett, and M. Alford, "Predetection Fusion: Resolution Cell Grid Effects," *IEEE Trans. on Aerospace and Electronic Systems*, Vol. 35, No. 3, 1999.

[8] C. Fang, et.al., "The Calculation and Analysis of the Bistatic Quantum Radar Cross Section for the Typical 2-D Plate", *IEEE Photonics Journal*, Vol. 10, No. 2, 2018.